RZ 3525 (# 99539) 01/12/04
Mathematics & Physics 9 pages

Research Report

Nonlinear Mechanical Coupling of Harmonic Oscillators Applied for a Vibrational AND Function

U. Dürig, O. Züger, A. Knoll, P. Vettiger, and G. Binnig

IBM Research GmbH
Zurich Research Laboratory
8803 Rüschlikon
Switzerland

Nonlinear Mechanical Coupling of Harmonic Oscillators Applied for a Vibrational AND Function

U. Dürig,* O. Züger,† A. Knoll, P. Vettiger, and G. Binnig
IBM Research, Zurich Research Laboratory, 8803 Rüschlikon, Switzerland

Abstract

This report describes a nonlinear mechanical coupling scheme for two perpendicular motions by means of a conventional spring. The nonlinear coupling scheme is applied for the design of a purely mechanical AND function that couples a superposition of two parallel input vibrations to an output oscillator that vibrates orthogonally to the input oscillators. The performance of the AND function was numerically simulated for a variety of coupling parameters and input amplitudes. Upper limits on the coupling strength were found for fixed input amplitudes, and, similarly, upper limits of the input amplitudes exist for fixed coupling parameters. Beyond these critical values, the motion of the output was found to become chaotic. A modified version of the AND function acting as a mechanical modulator was numerically investigated for application as a mechanical power amplifier. In a frequency up-converter configuration, a significant amplification of the vibrational power fed into the modulator can be achieved. The feasibility of the nonlinear mechanical coupling and its application for a vibrational AND function were demonstrated in an experimental setup.

I. INTRODUCTION

Given the limitations of the conventional semiconductor design of logic functions, alternative device concepts have been considered. At very small length scales, molecular [1] or even atomic [2] devices have been studied, whereas optical switching devices are needed for signal processing based on light [3].

In this paper, we explore the feasibility of a mechanical implementation of the AND function. The principle of operation is the nonlinear coupling of an output oscillator to two input oscillators.

The nonlinear coupling of mechanical oscillators is still an active field of interest regarding its application in dynamic vibration absorbers [4]. An effective way to mitigate vibrations in an oscillating structure is to couple a second oscillator to the structure. The danger of structural system failure can be reduced if an effective energy transfer from the structure to the absorber is established at the resonance frequency ω_0 of the primary structure.

If the second oscillator is coupled to the first in such a way that (i) the two oscillators represent two normal vibration modes of the system, (ii) the coupling between the two oscillators is nonlinear, and (iii) the lower resonance frequency is one half of the higher resonance frequency, then autoparametric resonance is established [5–7]. Under these conditions an effective energy transfer occurs from the exited structure to the second oscillator [6]. Recent examples of experimental studies of such systems can be found in [6, 7]. Parametric excitation of mechanical oscillators can also be used for amplification and noise squeezing of mechanical oscillations [8].

*Electronic address: drg@zurich.ibm.com
†Now at Unaxis Balzers Ltd., Division Optics, 9496 Balzers, Liechtenstein

For our purpose we use very similar concepts to establish the mechanical AND function and to optimize the energy transfer of the two input oscillators to the output oscillator. A purely nonlinear coupling to the output oscillator is established. A system with dimensions that are typical of a micromechanical implementation is studied numerically. In addition, a modified version of the AND function acting as a mechanical modulator is numerically investigated for application as a mechanical power amplifier. Finally, in an experimental setup, the feasibility of the nonlinear mechanical coupling and its application for a vibrational AND function are demonstrated.

II. NONLINEAR MECHANICAL COUPLING OF HARMONIC OSCILLATORS

Nonlinear effects in a system of coupled oscillators are usually obtained by driving the system at large amplitudes such that nonlinearities of the coupling potential become significant. An alternative way of realizing nonlinear coupling between oscillators is shown in Fig. 1. The oscillators vibrate in *orthogonal* directions, and a conventional spring couples the two motions of the oscillators. In contrast to the nonlinearities obtained for large vibration amplitudes, the nonlinear coupling between the orthogonal motions is already effective at small amplitudes.

The coupling potential U_c between the oscillators can be written as

$$U_c(z,y) = \frac{1}{2}k_c\left(\left(z^2+(l_c+y)^2\right)^{1/2}\right) - l_c\Big)^2 . \quad (1)$$

The force component in y-direction, F_y, is given by the y-component of the potential gradient ∇U_c:

$$F_y = \frac{\partial U_c}{\partial y} + k_c(l_c+y)\left(1 - \frac{l_c}{\left(z^2+(l_c+y)^2\right)^{1/2}}\right) . \quad (2)$$

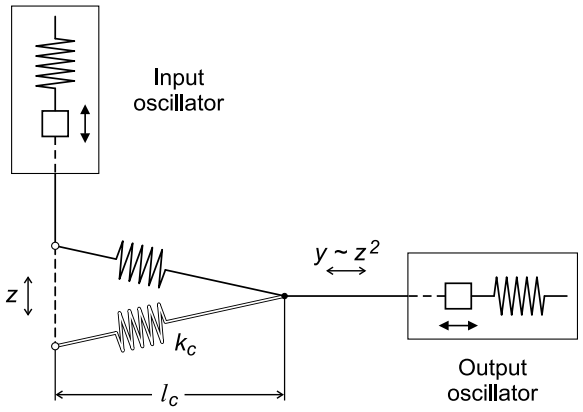

FIG. 1: Nonlinear mechanical coupling of orthogonal motions with a conventional spring.

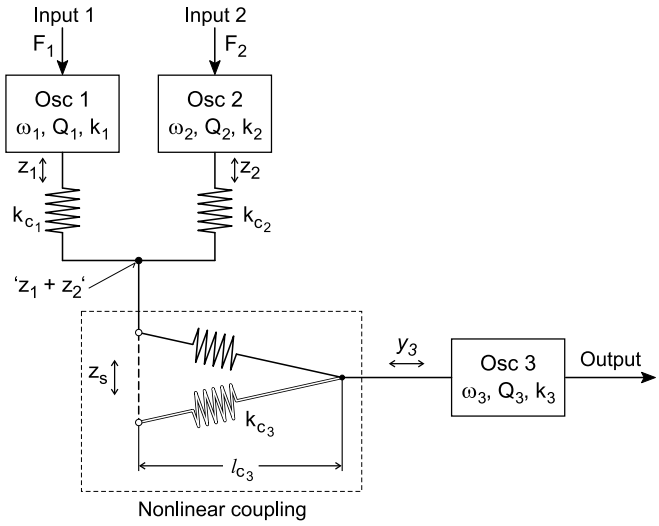

FIG. 2: Schematic of the vibrational AND function.

The lowest-order series expansion of the above expression [Eq. (2)] is

$$F_y = k_c \left(y + \frac{1}{2I_c} z^2 \right) . \tag{3}$$

The quadratic dependence of the force F_y on the z-position of the input oscillator reflects the nonlinear part of the coupling potential. A sinusoidal variation of z generates an oscillatory force in the y-direction at *twice* the frequency of the z-motion. The oscillator motion $z = A\sin(\omega t)$ of the input generates a second harmonic force $F_{yz} = k_c/4l_c \cos(2\omega t)$ acting on the output oscillator. Furthermore, the coupling spring adds a linear force component $F_{yc} = k_c\, y$ to the output oscillator, resulting in a shift $\Delta f = f_c(k_c/k)$ of its resonance frequency. Thus, in order to obtain a large vibration amplitude of the output oscillator, the resonance frequency of the output oscillator has to be adjusted at twice the input frequency, i.e., at 2ω.

III. VIBRATIONAL AND FUNCTION

The nonlinear coupling between oscillators can be used to implement a vibrational AND function. Two parallel input oscillators are linearly coupled by springs, and the resulting "sum" vibration is nonlinearly coupled to a third oscillator that vibrates perpendicularly to the input oscillators. A schematic of the AND function is shown in Fig. 2

The input oscillators Osc1 and Osc2 are excited to the vibration amplitudes z_1 and z_2, respectively. Both are coupled by springs to a common coupling point denoted as "$z_1 + z_2$" (more specifically, the forces from each oscillator are added at the coupling point). The stiffnesses of these springs are k_{c_1} and k_{c_2}, respectively. For equal stiffness, i.e., $k_{c_1} = k_{c_2}$, the motion z_s of the coupling point is proportional to the sum $z_1 + z_2$ of the two input amplitudes (see below). The motion z_s excites the output oscillator Osc3 through the nonlinear coupling generated by the spring having its axis perpendicular to the z-direction. The coupling spring has a stiffness k_{c_3} and a length l_{c_3} at zero force. The total coupling potential is

$$\begin{aligned} U_c(z_1, z_2, z_s, y_3) \;=\; & \frac{1}{2}k_{c_1}(z_1 - z_s)^2 + \frac{1}{2}k_{c_2}(z_2 - z_s)^2 \\ & + \frac{1}{2}k_{c_3}\left(\left(z_s^2 (l_c + y_3)^2\right)^{\frac{1}{2}} - l_c \right) . \end{aligned} \tag{4}$$

The motion z_s of the coupling point is determined by the constraint of zero total force in equilibrium, i.e., $\partial U_c/\partial z_s = 0$. For small amplitudes z_1, z_2 and y_3, this condition approximately yields $z_s = (k_{c_1} z_1 + k_{c_2} z_2)/(k_{c_1} + k_{c_2})$ For equal coupling springs $k_{c_1} = k_{c_2}$, this expression simplifies to $z_s = \frac{1}{2}(z_1 + z_2)$, reflecting the sum of the input amplitudes. Using this expression in Eq. (3) yields a force component that is proportional to the product $z_1\, z_2$ of the input vibration amplitudes

$$F_{y,z_1 \cdot z_2} = k_{c_3}\, \frac{1}{I_{c_3}}\, z_1\, z_2 \, . \tag{5a}$$

For the input vibrations $z_1 = A_1 \cos(\omega_1 t)$ and $z_2 = A_2 \cos(\omega_2 t)$, the corresponding force has a component oscillating with the frequency $\omega_1 + \omega_2$,

$$F_{y,\omega_1+\omega_2} = k_3\, \frac{1}{2}\, A_1\, A_2\, \cos\left((\omega_1 + \omega_2)t\right) . \tag{5b}$$

By choosing the resonance frequency ω_3 of the output oscillator such that it coincides with the sum frequency $\omega_1 + \omega_2$, the amplitude y_3 of the output oscillator becomes proportional to the product $A_1\, A_2$ of the input oscillators. Thus, the output oscillator only vibrates at its resonance frequency if there is a nonvanishing vibration amplitude at *both* input oscillators simultaneously.

IV. NUMERICAL SIMULATION OF THE VIBRATIONAL AND FUNCTION

A. Mathematical Model and Numerical Procedures

Based on the model in Fig. 2, the response of the vibrational AND function was numerically simulated for a variety of different coupling parameters k_{c_1}, k_{c_2}, k_{c_3}, and l_{c_3}, and input amplitudes z_1 and z_2. The differential equations describing the motion of the two input oscillators (Osc1, Osc2) and the output oscillator (Osc3) are

$$\ddot{z}_1 + \frac{\omega_1}{Q_1}\dot{z}_1 + \omega_1^2 z_1 + \frac{\omega_1^2}{k_1}\frac{\partial U_c}{\partial z_1} = \frac{\omega_1^2}{k_1}F_1\cos(\omega_{1s}t), \quad (6a)$$

$$\ddot{z}_2 + \frac{\omega_2}{Q_2}\dot{z}_2 + \omega_2^2 z_2 + \frac{\omega_2^2}{k_2}\frac{\partial U_c}{\partial z_2} = \frac{\omega_2^2}{k_2}F_2\cos(\omega_{2s}t), \quad (6b)$$

$$\ddot{y}_3 + \frac{\omega_3}{Q_3}\dot{y}_3 + \omega_3^2 y_3 + \frac{\omega_3^2}{k_3}\frac{\partial U_c}{\partial y_3} = 0\,, \quad (6c)$$

where ω_n is the (angular) resonance frequency of the corresponding oscillator, Q_n is the quality factor of the resonance, and k_n is the spring constant describing the coupling to the external driving force with amplitude F_n. The frequency of the driving force matches the resonance frequency of the coupled oscillator. The resonance frequency of the coupled oscillator, ω_{1s}, is shifted with respect to the resonance frequency ω_1 of the free oscillator according to the relation $\omega_{1s} = \omega_1\left(1 + k_1^{-1}\left(\partial^2 U_c\right)/\left(\partial z_1^2\right)\right)$. A corresponding expression relates ω_{2s} to ω_2 and ω_{3s} to ω_3. To excite the output oscillator at its resonance frequency ω_{3s}, the frequency ω_3 of the free oscillator is chosen such that the relation $\omega_{3s} = \omega_{1s} + \omega_{2s}$ is met for the actual coupling potential.

Starting from the initial positions $z_1 = 0$, $z_2 = 0$ and $y_3 = 0$ at $t = 0$, the differential equations (Eqs. (6a)-(6c)) are iteratively integrated for a time step dt by means of the Runge–Kutta algorithm [9]. Prior to each integration step, the position of the coupling point z_s is calculated from the zero-force condition $\partial U_c/\partial z_s = 0$ for the actual positions z_1, z_2, and y_3. During the iteration process, the mean absorbed power P_{a_1} and P_{a_2} of the input oscillators are calculated from the instantaneous energy flows $I_{E_1}(t) = F_1\cos(\omega_{1s}t)\dot{z}_1(t)$ and $I_{E_2}(t) = F_2\cos(\omega_{2s}t)\dot{z}_2(t)$ by filtering $I_{E_1}(t)$ and $I_{E_2}(t)$ with a second-order Butterworth low-pass filter having a cutoff frequency ω_{LP} of $20\omega_{1s}$. Similarly, the mean dissipated powers P_{d_1}, P_{d_2}, and P_{d_3} are calculated using equivalent low-pass filters with the same cutoff frequency. Because the output oscillator (Osc3) is driven only by the nonlinear coupling to the motion z_s of the coupling point, the absorbed power P_{a_3} in Osc3 is equal to the dissipated power P_{d_3} once the vibration amplitudes have reached a steady-state value. Thus, P_{d_3} reflects the amount of energy transferred from the input oscillators to the output oscillator.

The numerical simulations were performed assuming parameters that are typical of an AND function with micromechanical dimensions. The resonance frequencies were in the 1 kHz, and spring constants in the 10 N/m range. Specifically, the resonance frequency of the input oscillators were set to $\omega_1 = 1000$ Hz and $\omega_2 = 1400$ Hz; the spring constants were $k_1 = 10$ N/m and $k_2 = 16$ N/m, and the Q-factors were $Q_1 = Q_2 = 30$. The spring constants of the couplings to the coupling point were $k_{c_1} = k_{c_2} = 1$ N/m, inducing a resonance frequency shift of $+0.049$ for input oscillator 1 and $+0.029$ for input oscillator 2. The shifted resonance frequencies were then $\omega_{1s} = 1049$ Hz and $\omega_{2s} = 1441$ Hz. The resonance frequency of the output oscillator was set to $\omega_{3s} = \omega_{1s} + \omega_{2s} = 2490$ Hz by adjusting ω_3 for the actual parameter of the coupling spring constant k_{c_3}. The spring constant k_3 of the output oscillator is set [9] to 10 N/m. The Q-factor of the output oscillator was set to the same value as Q_1 and Q_2, namely, $Q_3 = 30$. In a realistic setup of a mechanical AND function, the coupling from the coupling point to the spring connecting to the output oscillator has a mechanical reduction (see Fig. 9 below). The motion of the coupling spring is reduced by the factor called r_{c_3}, i.e., y_3 in the coupling potential U_c is replaced by the expression $r_{c_3}\, y_3$. For the simulations described here, the reduction factor was set to $r_{c_3} = 0.2$.

B. Coupling Efficiency for Various Coupling Parameters

The coupling efficiency from the inputs to the output was explored by varying the parameters k_{c_3} and l_{c_3} from 1 to 1000 N/m and 5 to 300 um, respectively. The input force amplitudes F_1 and F_2 were chosen such that the resulting vibration amplitudes z_1 and z_2 were between 0.001 and 3 μm. The performance of the AND function was analyzed both by the power transfer efficiency $\eta = P_{d_3}/(P_{a_1} + P_{a_2})$ and the amplitude gains $g_1 = y_{3\,\mathrm{rms}}/z_{1\,\mathrm{rms}}$ and $g_2 = y_{3\,\mathrm{rms}}/z_{2\,\mathrm{rms}}$. True rms values were calculated because of the significant nonharmonic contributions to the vibration amplitude $y_3(t)$. Both the power values and the amplitude values were calculated after an integration time τ_i of about 60 ms. This time period corresponds to about six times the slowest response-time constant in the system, i.e., the response time of input oscillator 1, which is $\tau_1 = 2Q_1/\omega_1 = 9.1$ ms. The integration step width, dt, was determined by dividing the oscillation period of the fastest oscillator in the system, i.e., the output oscillator Osc3, into 50 equal steps. The resulting time-step width was $dt \simeq 7\,\mu$s.

Figure 3 shows the power transfer efficiency η and the output vibration amplitude $y_{3\,\mathrm{rms}}$ as a function of the length scale l_{c_3} for various stiffnesses k_{c_3} of the coupling spring. The input amplitudes were $z_1 = z_2 = 0.7\,\mu\mathrm{m}_{\mathrm{rms}}$. The power transfer efficiency η has a maximum of $\simeq 0.1$ for $k_{c_3} = 1000$ N/m at $l_{c_3} \simeq 50\,\mu$m. For these parameters, up to 10% of the input power can be transferred

to the output oscillator. The vibration amplitude $y_{3\,\mathrm{rms}}$ of the output oscillator has a maximum. Position and height of the maximum depend on the coupling constant k_{c_3}. For small values of k_{c_3}, the position of the maximum appears to be below $l_{c_3} = 5\,\mu$m and the height reaches values slightly larger than $y_{3\,\mathrm{rms}} = 0.15\,\mu$m; for $k_{c_3} > 100$ N/m, the position of the maximum moves to values of $l_{c_3} > 10\,\mu$m, whereas the height decreases to less than $y_{3\,\mathrm{rms}} = 0.1\,\mu$m.

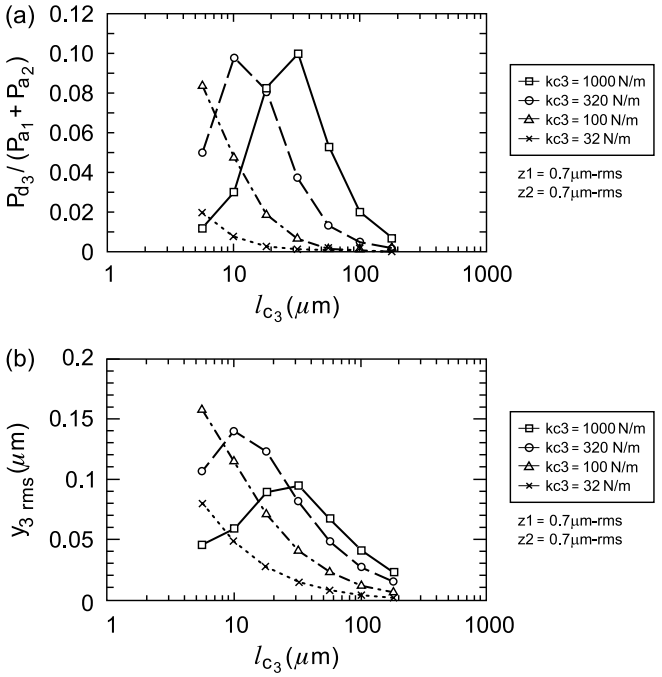

FIG. 3: (a) Power transfer efficiency and (b) output vibration amplitude for a variable length l_{c_3} of the nonlinear coupling at various stiffnesses k_{c_3} of the coupling spring.

If the length l_{c_3} is reduced to less than 5 μm or the stiffness k_{c_3} of the spring increased to values above 1000 N/M, the amplitude y_3 of the output will no longer attain a steady-state value but become chaotic. Thus, its detection after a fixed integration time is meaningless for the characterization of the coupling efficiency η and of the amplitude gains g_1 and g_2. These limits for l_{c_3} and k_{c_3} for achieving a steady-state output amplitude are only valid for the input amplitudes $z_1 = z_2 = 0.7\,\mu\mathrm{m_{rms}}$; for larger (smaller) amplitudes, the lower limit for l_{c_3} becomes larger (smaller) and the upper limit for k_{c_3} becomes smaller (larger).

C. Coupling Efficiency for Variable Input Amplitudes

Owing to the nonlinearity of the coupling, the output amplitude does not *a priori* scale with the input amplitudes. For this reason, the dependence of the output amplitude y_3 on the input amplitudes z_1 and z_2 was investigated for fixed parameters l_{c_3} and k_{c_3} of the nonlinear coupling. The values of these parameters were chosen such that the power transfer was maximum for the input amplitudes $z_1 = z_2 = 0.7\,\mu\mathrm{m_{rms}}$, i.e., $l_{c_3} + 20\,\mu$m and $k_{c_3} = 300$ N/m. Figure 4(a) shows the dependence of the power transfer efficiency $\eta = P_{d_3}/(P_{a_1} + P_{a_2})$ on z_1 for various values of z_2. As expected for an AND function, the maximum output power is obtained if a large signal amplitude is applied to both inputs. If at least one of the inputs has a low amplitude, the output power is reduced significantly. Figure 4(b) shows the output/input amplitude gain $g_1 = y_{3\,\mathrm{rms}}/z_{1\,\mathrm{rms}}$ with the other input amplitude z_2 on a constant level. For small z_2, the gain g_1 stays constant for small z_1 and becomes larger as z_1 is increased to more than 0.5 μm. For large z_2, however, the gain g_1 *decreases* as the amplitude z_1 is increased, which contradicts a proper operation of the AND function.

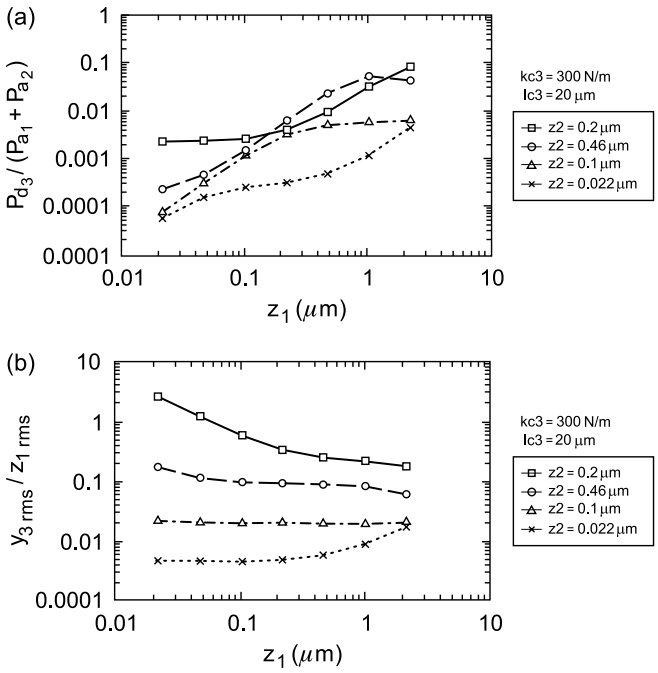

FIG. 4: (a) Power transfer efficiency and (b) output vibration amplitude for varying input amplitudes z_1 and z_2.

For the range of input vibration amplitudes investigated here, the output amplitude reaches a stable value at the end of the integration time ($\sim$ 60 ms) for any combination of the two amplitudes z_1 and z_2. For larger amplitudes, however, the output amplitude no longer becomes stable, and its time evolution becomes chaotic.

D. Bias Stress on Coupling Spring

In the model used so far, the spring of the nonlinear coupling was assumed to have zero stress when the input

amplitudes z_1 and z_2 were zero. However, this assumption is not a necessary restriction for the nonlinear coupling. If a bias stress $F_b = k_{c3} y_b$ is applied to the spring, the coupling potential is modified slightly by replacing y_3 with the expression $y_3 + y_b$ in Eq. (4). As a consequence, the initial position of y_3 at $t = 0$ no longer is $y_{3,0} = 0$. The position $y_{3,0}$ is determined by the condition of the static equilibrium $\partial U_c/\partial y_3 + k_3 y_3 = 0$ for $z_1 = z_2 = 0$.

The coupling potential changes fundamentally when a bias stress is applied to the coupling spring. Figure 5 shows the potential as a function of the position of the sum point z_s for either compressive ($y_b < 0$) or expansive bias stress ($y_b > 0$). For expansive stress, the curvature of the potential at $z_s = 0$ increases, resulting in a positive shift of the resonance frequency. For compressive stress, however, the potential splits into two equivalent minima. For small amplitudes of z_s, the motion is confined to either one of the two minima where the system initially was at $t = 0$. For larger amplitudes, however, the system can exceed the barrier at $z_s = 0$, initiating a sudden increase of the vibration amplitude z_s as the input amplitude is increased. As a consequence, the excitation of the output oscillator rises accordingly and results in a significant increase of the amplitude y_3.

This highly nonlinear behavior is reflected in the transfer efficiency η and the amplitude gains g_1 and g_2 of the AND function. Figure 6 shows the power transfer efficiency η in (a) and the amplitude gain g_1 in (b) for four different compressive stress bias values y_b. For no or low compressive stress ($y_b = 0, -2\,\mu$m), the power transfer in (a) continuously increases and the amplitude gain in (b) becomes slightly smaller as the input amplitude z_1 is increased. Above a critical amplitude $z_1 \simeq 3\,\mu$m, the coupling efficiency η drops slightly and increases again for larger values of z_1. For $y_b = -4\,\mu$m, however, the power transfer to the output oscillator is almost independent of z_1; the output is driven by the second input oscillator only. For this specific bias stress, the input amplitude $z_2 = 1\,\mu$m is large enough to raise the energy of the system above the potential barrier at $z_s = 0$, see Fig. 5, and enables a large oscillation of z_s between the two branches of the potential curve. This behavior is also reflected in the amplitude gain curve in Fig. 6(b). The slope of -1 for $y_b = -4\,\mu$m reflects the independence of the output amplitude $y_{3\,\mathrm{rms}}$ of the input for small values of z_1. For a slightly larger compressive stress of $y_b = -6\,\mu$m, the output amplitude y_3 abruptly increases for a narrow range of input amplitudes z_1 above 1 μm.

Compressive stress on the coupling spring could be used to obtain significantly larger output vibration values for the same input levels. Furthermore, because of the pronounced nonlinearity for a specific range of input amplitudes, compressive stress could be used to set a threshold for the input amplitudes to generate a detectable output signal. However, in both cases, the bias stress has to be accurately tuned to obtain the specific properties. In a micromechanical device, this might be a difficult if not even impossible requirement to fulfill.

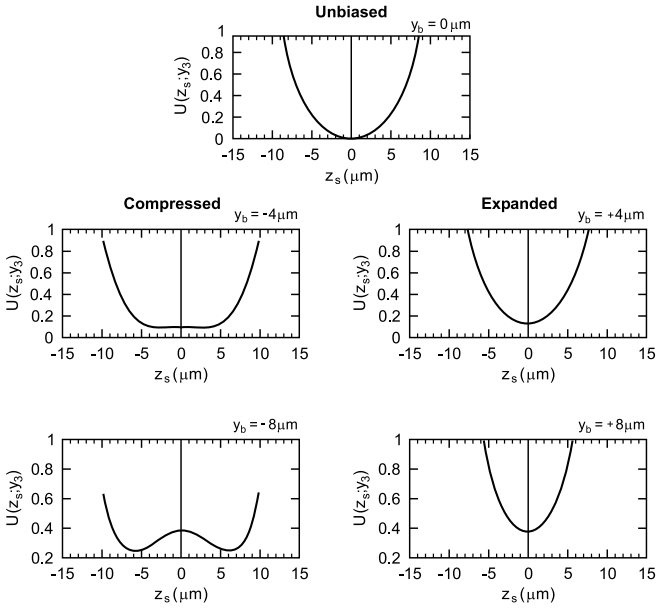

FIG. 5: Total potential U as a function of the "sum point" coordinate z_s for either compressive ($y_b < 0$) or expansive bias stress ($y_b > 0$) applied to the coupling spring.

V. MECHANICAL POWER AMPLIFICATION

The nonlinear coupling of the two input oscillators to a third output oscillator can be viewed as an amplitude-mixing element for vibrations. One of the inputs acts as the high-frequency carrier input, the other is the low-frequency modulator input. The nonlinear coupling generates an oscillatory force at both the sum frequency (upper sideband) and the difference frequency (lower sideband) of the input oscillators. In the case of negligible loss in the nonlinear coupling, the power transfer to the output is governed by some fundamental relations called the Manley–Rowe equations [10]. Neglecting higher-order sidebands, these equations are as follows. For the upper sideband $\omega_c + \omega_1$

$$\frac{P_c}{\omega_c} + \frac{P_+}{\omega_c + \omega_1} = 0 \tag{7a}$$

$$\frac{P_1}{\omega_1} + \frac{P_+}{\omega_c + \omega_1} = 0 \tag{7b}$$

and for the lower sideband $\omega_c - \omega_1$

$$\frac{P_c}{\omega_c} + \frac{P_-}{\omega_c - \omega_1} = 0 \tag{8a}$$

$$\frac{P_1}{\omega_1} - \frac{P_-}{\omega_c - \omega_1} = 0\,. \tag{8b}$$

P_c and P_1 denote the power absorbed at the carrier input and at the modulator input, respectively, and ω_c and ω_1

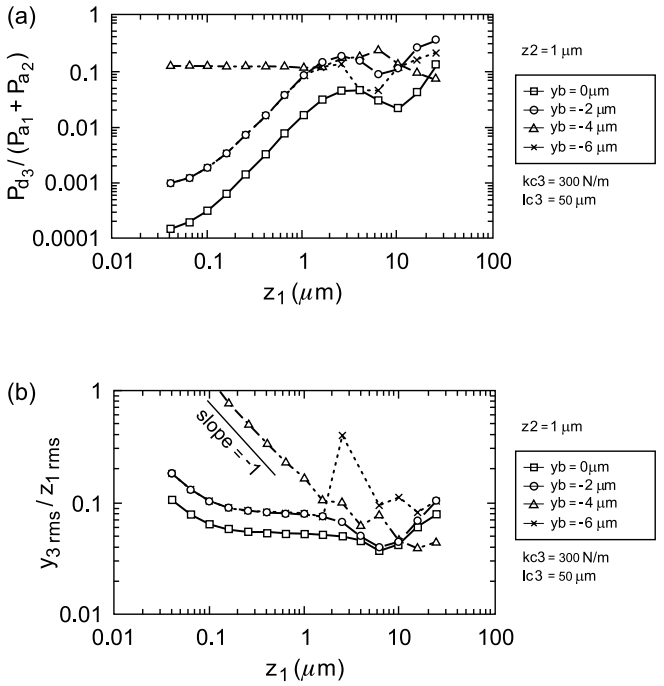

FIG. 6: (a) Power transfer efficiency and (b) amplitude gain as a function of input amplitude z_1 for fixed input amplitude z_2. For $y_b = -4\,\mu$m and small input amplitude z_1, the output amplitude is independent of z_1. The output is driven by the input amplitude z_2.

are the corresponding frequencies. The power transferred to the upper and lower sideband is $-P_+$ and $-P_-$, respectively (note that *absorbed* powers are positive). Rewriting Eq. (7b), the power gain $G_+ = -P_+/P_1$ in the upper sideband is given by $G_+ = (\omega_c+\omega_1)/\omega_1$. For a large carrier frequency $\omega_c \gg \omega_1$, the gain is approximately given by $G_+ = \omega_c/\omega_1$, and the output power rises linearly with the carrier frequency ω_c.

For the lower sideband, however, the power gain is negative, i.e., $G_- = -P_-/P_1 = -(\omega_c - \omega_1)/\omega_1 < 0$. Because the output emits power, P_- is negative by convention, and because $G_- < 0$, also the input power P_1 must be negative. Accordingly, there is a power flow *from* the carrier input *via* the output oscillator *to* the modulator input. Thus, the modulator input oscillator can be excited without any signal being applied to the modulator input. The tendency to self-oscillations renders the lower sideband amplifier potentially unstable.

The performance of the upper sideband amplifier was simulated by means of the same procedure as for the vibrational AND function. Unlike the AND function, however, the resonance frequency of one of the inputs was varied to investigate the power gain for various carrier frequencies f_c. Figure 7(a) shows the power gain $G_+ = P_{d_3}/P_{a_1}$ as a function of the modulator input amplitude z_1 for various carrier frequencies f_c and for a fixed carrier input amplitude $z_2 = 2.2.\,\mu$m. For low input amplitudes z_1, the power gain varies as z_1^{-2}, indicating a constant output amplitude, whereas the input power rises as z_1^2. For input amplitudes in the range $z_1 = 0.1$ to $2\,\mu$m, the power gain G_+ is independent of z_1, as demanded for a linear amplifier. Above $z_1 \simeq 2\,\mu$m, the carrier amplitude z_c is smaller than the modulator amplitude z_1, and the output amplitude is dominated by the absorbed power at the modulator input. As a consequence, G_+ drops as z_1 is increased further.

The amplitude gain $g_+ = y_{3\,\mathrm{rms}}/z_{1\,\mathrm{rms}}$ of the upper sideband modulator is shown in Fig. 7(b). The linear drop of g_+ for small input amplitudes indicates that the output amplitude y_3 is independent of the modulator input amplitude z_1. The amplitude gain is constant in the range $z_1 = 0.1$ to $2\,\mu$m and drops at $z_1 > 2\,\mu$m, reflecting the corresponding behavior of the power gain G_+ at these input amplitudes z_1.

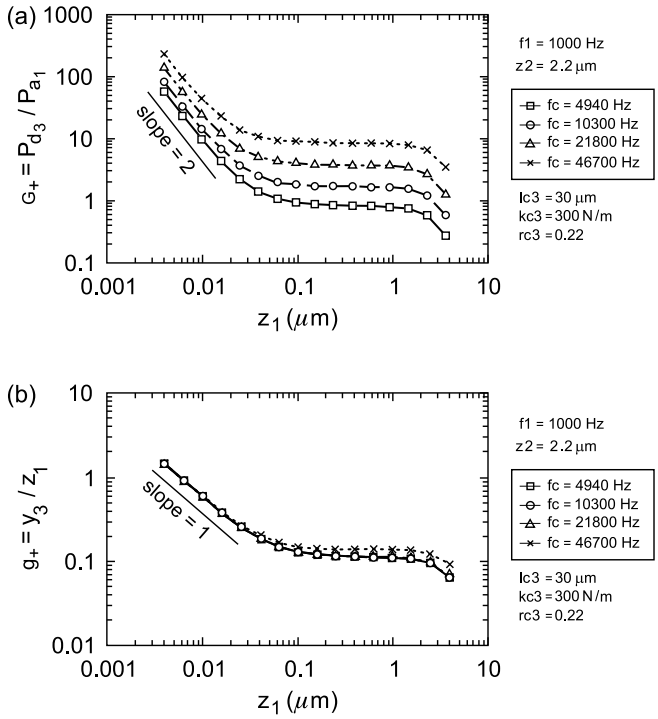

FIG. 7: (a) Power gain G_+ and (b) amplitude gain g_+ of the upper sideband modulator for a variable modulator input amplitude z_1 and for various carrier frequencies f_c and constant carrier input amplitude $z_c = 1\,\mu$m. Constant power gain G_+ is achieved for input amplitudes in the range $z_1 = 0.1$ to $2\,\mu$m.

Unlike the power gain G_+, however, the amplitude gain g_+ is almost independent of the carrier frequency f_c.

The power gain G_+ increases wit larger f_c, as shown in Fig. 8 for various carrier amplitudes z_c. The dependence of G_+ on f_c is almost linear, as predicted by the Manley–Rowe equations, (7a) and (7b). For these equations, the entire power output was assumed to be confined to the upper sideband. In reality, however, the nonlinear coupling transfers power into other frequency components such as the multiple harmonics of the input frequencies ($2\omega_1$, $2\omega_c$, $3\omega_1$, $3\omega_c$, ...) higher-order sidebands

($\omega_c \pm 2\omega_1$, $\omega_c \pm 3\omega_1$, ...). As a result, the magnitude of the power in the upper sideband $\omega_c + \omega_1$ is smaller than what is expected from the (simplified) Manley–Rowe equations [(7a), (7b) and (8a), (8b)].

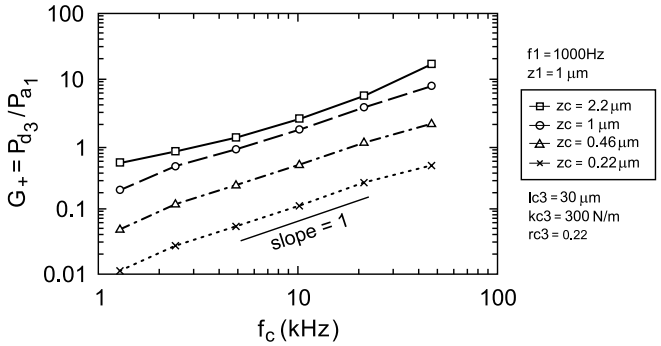

FIG. 8: Power gain G_+ of the upper sideband modulator for variable carrier frequency f_c and various carrier amplitudes z_c. The modulator frequency is $f_1 = 1000$ Hz, and the input amplitude is $z_1 = 1\,\mu$m. G_+ increases linearly with f_c.

VI. NONLINEAR COUPLING WITH INTERNAL RESONANCES

In the numerical simulations of the AND function and the power amplifier described above, all couplings between the oscillators were assumed to have zero mass and, consequently, no internal resonances. In a real system, however, the coupling springs have internal resonances. Yet for a well-designed system, these resonance frequencies are significantly higher than the frequencies of the oscillators. In this case, the model with no or infinitely high resonance frequencies is a good approximation.

In a more realistic model of the vibrational AND function, a finite mass m_s is added to the coupling. The mathematical model describing the dynamics of the system (Eqs. (5a)–(5c)) is extended by a differential equation for the motion of the mass m_s.

$$\ddot{z}_s + \frac{\omega_s}{Q_s}\dot{z}_s + \omega_s^2 z_s + \frac{\omega_s^2}{k_{c_1} + k_{c_2}}\frac{\partial U_c}{\partial z_s} = 0\,. \qquad (9)$$

Instead of using the not well-defined mass m_s of the coupling to characterize the internal dynamics of the coupling, the resonance frequency ω_s of the coupling is used in Eq. (9). This equation replaces the condition $\partial U_c/\partial z_s = 0$ used in the preceding sections to determine the position z_s.

For the numerical simulation of the AND function with variable internal resonance frequency ω_s, similar parameters as in Sect. IV were used for the coupling springs, namely, $k_{c_1} = k_{c_2} = 1/$ N/m, $k_{c_3} = 500$ N/m, $r_{c_3} = 0.2$, and $l_{c_3} = 30\,\mu$m. The resonance frequencies of the uncoupled input oscillators were $f_1 = 1000$ Hz and $f_2 = 1650$ Hz, respectively. The coupling shifted the resonance frequencies by +49 and +38 Hz, yielding $f_{1s} = 1049$ Hz and $f_{2s} = 1688$ Hz. The output oscillator frequency then was $f_{3s} = f_{1s} + f_{2s} = 2737$ Hz. The Q-factors had equal values, $Q_1 = Q_2 = Q_3 = 50$. For the internal resonance of the coupling system, negligible loss was assumed by using a large Q-factor $Q_s = 10^4$.

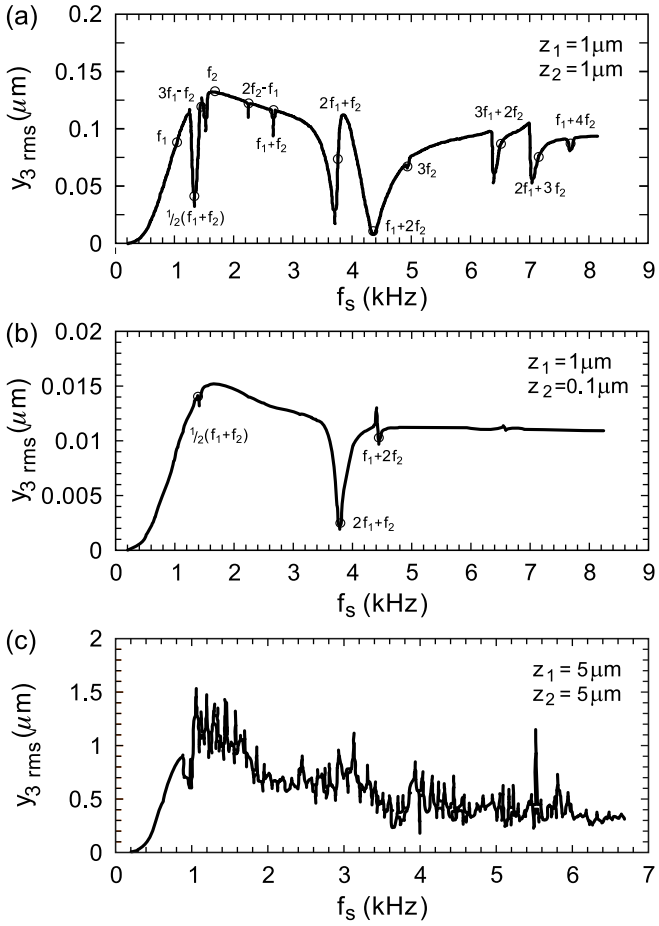

FIG. 9: Output amplitudes of the vibrational AND function with variable internal resonance frequency of the nonlinear coupling. (a) Input amplitudes $z_1 = z_2 = 1\,\mu$m; (b) $z_1 = 1\,\mu$m, $z_2 = 0.1\,\mu$m, and (c) $z_1 = z_2 = 5\,\mu$m. Multiples of the input frequencies are marked in the plots (for the sake of simplicity, the index "s" has been omitted).

The internal resonance frequency f_s was varied from 200 to 8200 Hz for three different input amplitudes. Figure 9(a) shows the output vibration amplitude as a function of f_s of the coupling for the input amplitudes $z_1 = z_2 = 1\,\mu$m. The output amplitude y_3 varies by more than a factor of ten for different resonance frequencies of the coupling. Characteristic amplitude peaks and dips occur at multiples of the resonance frequencies f_1 and f_2 of the inputs and the outputs (for the sake of simplicity, the index "s" denoting the shifted resonance frequencies is omitted in this section). At reduced input amplitudes ($z_1 = 1\,\mu$m and $z_2 = 0.1\,\mu$m), most of the

peaks and dips disappear, and for a high internal resonance frequency, the amplitude levels off at a well-defined plateau (Fig 9(b)). For larger input amplitudes however ($z_1 = z_2 = 5\,\mu$m), the motion of the output oscillator becomes chaotic and the output amplitude spectrum is very noisy (Fig. 9(c)). The magnitude of the output amplitude is no longer predictable, making the AND function inapplicable.

This sections points to a severe problem for the design of an AND function based on nonlinear mechanical coupling. In order to achieve a high coupling efficiency of the output, the stiffness of the spring has to be on the order of magnitude of the spring constants of the oscillators. The high stiffness is achieved by using a bulkier geometry of the springs. As a consequence of the larger mass of the spring, the internal resonance frequencies of the coupling drop, making the output amplitude critically depend on the actual internal resonance frequency at vibration amplitudes that are still below the critical values for chaotic behavior. At larger amplitudes, the output amplitude no longer reaches a stable value. Thus, in order to achieve a proper functioning of the AND function, the inputs have to have a built-in amplitude limiter or the amplitudes have to be detected independently so as to trigger an overload warning if their magnitudes are too large.

VII. MACROMECHANICAL MODEL OF THE VIBRATIONAL AND FUNCTION

The feasibility of the nonlinear mechanical coupling scheme was tested on a macromechanical model of a vibrational AND function. The experimental setup is shown in Fig. 10. Aluminum cantilevers with a thickness $t = 0.5$ mm and a width $w = 8$ mm act as input and oscillators. The lengths of the two input cantilevers were $l_1 = 45$ mm and $l_2 = 33$ mm, respectively. The output cantilever at the higher frequency had a length of $l_3 = 25$ mm. The coupling between the inputs was V-shaped and cut from stainless steel foil having a thickness of 0.2 mm. The lengths of the two legs were $l_{c_1} = 20$ mm and $l_{c_2} = 15$ mm, respectively, and the width was 2.5 mm. The nonlinear coupling spring was made from the same foil and was S-shaped, making the spring stiff in the direction of the input vibration and soft in the direction of the output vibration. The length of the unloaded spring was $l_{c_3} = 20$ mm.

The spring constants of the cantilevers were estimated from the dimensions using the formula $k = (1/4)Ew(t/l)^3$, where E is Young's modulus. For the levers we obtained $k_1 = 200$, $k_2 = 500$ and $k_3 = 1100$ N/m, and for the couplings $k_{c_1} = 120$, $k_{c_2} = 300$ and $k_{c_3} = 2300$ N/m. The resonance frequencies of the input cantilevers were $f_1 = 202$ and $f_2 = 259$ Hz, with the Q-factors $Q_1 = 230$ and $Q_2 = 200$. The frequency of the output oscillator was adjusted to match the condition $f_3 = f_1 + f_2$, i.e., $f_3 = 461$ Hz. The corresponding Q-factor was $Q_3 = 120$.

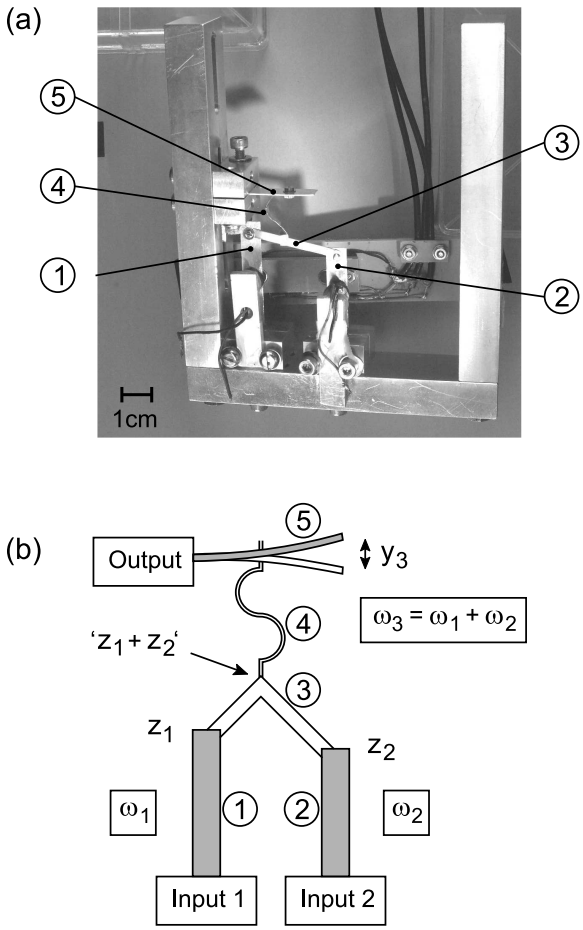

FIG. 10: Experimental setup of the vibrational AND function.

The cantilevers were excited by the magnetic force between a small permanent magnet glued onto the cantilevers and a small coil located close to the magnet. The vibration signal of the cantilevers was detected by miniature microphones located about 2 mm away from each cantilever. The output AC voltage from the microphones was calibrated by using a large excitation of the cantilevers and measuring the resulting vibration amplitude with an optical microscope.

Figure 11 shows the output amplitudes detected as input 1 is varied from about 20 to 400 μm for a set of different amplitudes of input 2. The output amplitude increases almost linearly (slope = 1) with the input amplitudes, indicating that the AND function is driven below the chaotic limit. For large input amplitudes on both inputs, the resulting output amplitude reaches a vibration amplitude of as much as several 100 μm. Thus, a significant fraction of the power adsorbed at the inputs is transferred to the output, indicating that the nonlinear coupling is rather strong.

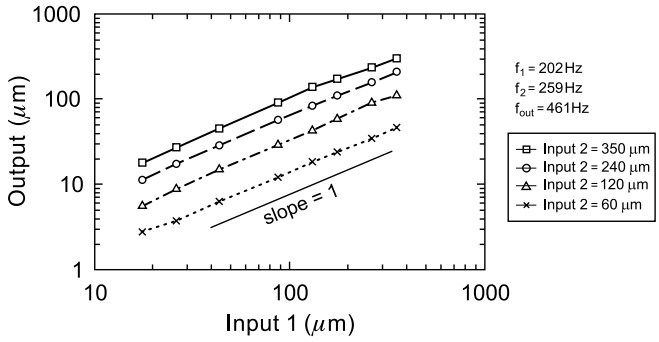

FIG. 11: Output vibration amplitude of the macroscopic model of the vibrational AND function as one of the input amplitudes is varied and the other kept constant.

VIII. CONCLUSION

We have demonstrated the feasibility of a mechanical AND function by means of nonlinearly coupled oscillators. Two input oscillators are coupled to a orthogonally vibrating output cantilever by a coupling spring, which results in an effective nonlinear coupling already at small amplitudes. The functionality of the system was demonstrated in an experimental setup and studied numerically.

The equations describing the system have been solved numerically for parameters typical of a mechanical realization with micromechanical dimensions. The power transfer efficiency η and the amplitude gains g_1 and g_2 were explored as a function of input amplitudes and coupling parameters with or without an additional bias stress on the coupling spring.

For moderate input amplitudes and optimized coupling parameters, the power transfer efficiency increases with increasing amplitudes and reaches a maximum of $\eta \approx 0.1$. If at least one of the inputs has a low amplitude, the output power is reduced significantly, as required for an AND function. Upper limits on the coupling strength were found for fixed input amplitudes, and, similarly, upper limits of the input amplitudes exist for fixed coupling parameters. Beyond these critical values, the motion of the output was found to become chaotic. An appropriate compressive bias stress on the coupling spring could be used to obtain significantly larger output amplitudes and to set a threshold for the input amplitudes in order to generate a detectable output signal. However, the bias stress has to be accurately tuned, which might be difficult to achieve in a micromechanical implementation.

The same setup can be viewed as a mechanical power amplifier. A low frequency modulator signal at one of the inputs can be amplified by supplying a high frequency carrier signal to the other input. If the output oscillator is tuned to the sum frequency of the two input oscillators, a power gain independent of the input amplitude can be established for a certain range of input amplitudes.

Acknowledgments

The authors gratefully acknowledge Heini Rohrer and Pierre Guéret for stimulating discussions.

[1] F. M. Raymo, *Adv. Mater.*, **14**, 401 (2002).
[2] A. J. Heinrich, C. P. Lutz, J. A. Gupta, and D. M. Eigler, *Science* **298**: 1381 (2002)
[3] see for example J. S. Aitchison, A. Villeneuve, G. I. Stegeman *Opt. Lett.* **20**: 698 (1995)
[4] J. Q. Sun, M. R. Jolly, M. A. Norris, *Journal of Mechanical Design* **117**, 234 (1995).
[5] A. Tondl, M. Ruijgrok, M. Verhulst, R. Nabergoj, *Autoparametric Resonance in Mechanical Systems* (Cambridge University Press, 2000).
[6] O. Cuvalci, A. Ertas, S. Ekwaro-Osire, I. Cicek, *Journal of Sound and Vibration* **249**, 701 (2002).
[7] I. Cicek, A. Ertas, *Mechanical Systems and Signal Processing* **16**, 1059 (2002).
[8] D. Rugar, P. Gruetter, *Phys. Rev. Lett.* **67**, 699 (1991).
[9] See, for example, P. Henrici, *Elements of Numerical Analysis* (John Wiley, New York, 1964), p. 274.
[10] J. M. Manley and H. E. Rowe, *Proc. IRE* **44**, 094 (1956).